Electron capture and deprotonation processes observed in collisions between Xe^{8+} and multiply protonated cytochrome-C

Serge Martin, C. Ortega, L. Chen, Richard Bredy, Arnaud Vernier, Philippe Dugourd, Rodolphe Antoine, Jérôme Bernard, G. Reitsma, O. Gonzalez-Magana, et al.

Electron capture and deprotonation processes observed in collisions between Xe^{8+} and multiply protonated cytochrome-C

S. Martin,[1,*] C. Ortega,[1] L. Chen,[1] R. Brédy,[1] A. Vernier,[1] P. Dugourd,[1] R. Antoine,[1] J. Bernard,[1] G. Reitsma,[2] O. Gonzalez-Magaña,[2] R. Hoekstra,[2] and T. Schlathölter[2]

[1]*Institut Lumière Matière, UMR5306 Université Lyon 1-CNRS, Université de Lyon, 69622 Villeurbanne cedex, France*

[2]*KVI Atomic and Molecular Physics, University of Groningen, Zernikelaan 25, NL-9747 AA Groningen, The Netherlands*

(Received 2 July 2013; revised manuscript received 19 December 2013; published 13 January 2014)

Electron-transfer processes in interaction between highly charged ions and multiply protonated proteins have been studied. Collisions between Xe^{8+} at 96 keV and protonated cytochrome-C at selected charge state (q from 15+ to 19+) result in mass spectra composed mainly of intact molecular ions. From the spectra, single and double electron capture processes by Xe^{8+} from the protonated molecular ions were identified and the relative cross sections were measured. An unexpected process, the deprotonation process, was also observed. It is tentatively attributed to the loss of a proton induced by the strong electric field carried by the projectile ion in long-distance collisions. Upon charge variation of the molecular target from 15 to 19, the single and double electron capture cross sections remain nearly constant, while the relative cross section of the deprotonation process increases dramatically from 0.8% (±0.1%) to 17% (±1%). This strong charge dependency is explained by the decrease of the proton affinities with the charge. This proton removal process has not been observed previously. It seems to be specific to the long-distance Coulomb interactions between protons bound along the protein chain and the highly charged atomic ions.

DOI: 10.1103/PhysRevA.89.012707 PACS number(s): 34.50.−s, 36.40.Qv, 34.10.+x, 36.40.Wa

I. INTRODUCTION

For many decades, collision dynamics between highly charged ions (HCIs) and atomic or molecular targets in the gas phase have been investigated [1]. Most works on ion-neutral target collisions were performed in crossed beam configurations while a number of more recent studies have employed merged beam techniques [2,3]. Ion-molecular target collisions have been investigated intensively during recent years in order to gain structural information of (eventually multiply) charged molecules and to study their stability and fragmentation dynamics. In these experiments, the electron transfer from the target molecule to the HCI is the main interaction mechanism leading to ionization, excitation, and the subsequent dissociation of the molecules. Most of the molecules investigated so far could be easily brought into the gas phase by evaporation using a simple oven [4–8]. An entire class of molecules of biological interest, including DNA bases, sugars, small amino acids, porphyrins, etc. [9–13], has been studied in collisions with HCIs. To bring larger and generally more fragile biomolecules into the gas phase, more sophisticated molecular source techniques such as electrospray ionization (ESI) have to be employed. Recently, an experimental setup combining an ESI, a radiofrequency (RF) ion trap device, and a HCI source has been built at the Zernike-LEIF facility at the Kernfysisch Versneller Instituut (KVI), University of Groningen. This experimental investigation of collisions between HCIs and stored small protonated peptides (Leucineenkephaline, bradykinin . . .) [14] has revealed two main classes of interaction processes: (i) electron capture processes at long collision distance leading to little excitation of the target and even formation of intact peptide dications; (ii) collisions at closer distance leading to higher energy deposition and extensive fragmentation of the peptide. This pioneering work has opened the way for exploring a new research field on interactions between HCIs and larger biomolecules such as proteins.

Electron transfer in ion-ion collisions at much lower interaction energies (a few eV) has already been studied intensively using ion trap mass spectrometry. Experimental techniques such as electron-transfer dissociation (ETD) and negative ETD are now routinely used for analytical purposes [15–20]. Gas phase charge transfer processes involving protonated peptides or proteins are directly related to the proton or electron binding energies of such species [21,22]. To measure these binding energies, photoionization (e.g., using synchrotron radiation) and electron impact ionization techniques have been employed [21–24]. As expected, for a given protonated protein the ionization potential (I_p) and electron affinity (EA) were found to depend sensitively on the charge q, i.e., the number of protons bound to the protein. For example, for a series of small proteins with mass between 1000 and 3500 amu (insulin, melittin), the I_p follows a simple linear law with q, I_p (eV) $= 9.8 + 1.1q$ [25]. For larger proteins such as cytochrome-C (denoted as cyt-C hereafter) ($m \approx 12 \times 10^3$ amu), the charge effect on the I_p is weaker and the linear q-dependent term is approximately $0.2q$ (eV) [23]. Besides the roughly linear variation feature of I_p as a function of q, Giuliani *et al.* [26] observed a small plateau in the $I_p(q)$ curve for protonated cyt-C, corresponding to structural modifications of the protein as demonstrated by Clemmer and Jarrold using ion mobility spectrometry [27].

In this paper, we study collisions between HCI Xe^{8+} at 96 keV and a multiply protonated biomolecule, the protein cyt-C, with charge state or the number of protons ranging from $q = 15+$ to 19+. The goal of this study is to address the electron transfer and relaxation mechanisms occurring in fast interactions involving two highly charged species. Single and double electron transfer from the highly charged

*Corresponding author: smartin@univ-lyon1.fr

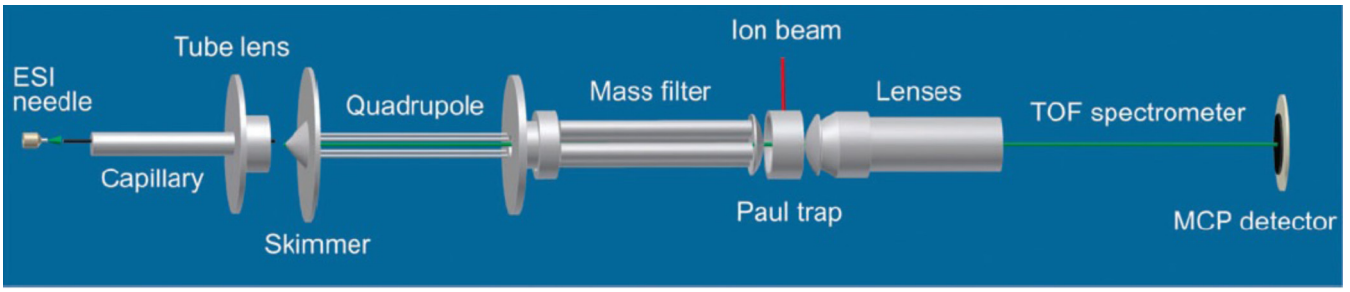

FIG. 1. (Color online) Experimental setup.

protein to a point-charge projectile ion was observed. The total electron-transfer cross section was calculated with the classical over-the-barrier model under the assumption of a simple linear molecular conformation. An unexpected process, the deprotonation process, was also observed. The charge dependency of its measured cross section was found strongly correlated to the proton affinity (the minimum energy to remove a proton from the molecule) of the protonated cyt-C.

II. EXPERIMENT

The experimental setup (Fig. 1) has been described in detail elsewhere [28] and only a short description is presented here. A homemade ESI source was used to produce the protonated molecules. A 30-μM methanol solution with typically 1% acetic acid contained bovine cyt-C molecules, denoted M, of mass 12 229 amu (Sigma-Aldrich). It was dispersed by electrospray into fine aerosols through a capillary heated to 100 °C. After solvent evaporation in vacuum, protonated molecular ions, denoted $[M + q\mathrm{H}]^{q+}$ with q ranging from 12+ to 20+, were formed with the attachment of q protons on the basic residues of the cyt-C. The density of free protons available in the solution could be controlled by varying slightly the density of the acetic acid. The higher the acid amount, the higher the proton density and therefore the higher the charge state q attained by the protonated molecules from the ESI source. The ions were guided by a first quadrupole and selected in charge state through a second quadrupole which served as a mass filter. The selected ions cyt-C $[M + q\mathrm{H}]^{q+}$ were then accumulated during about 500 ms in a Paul trap where a He buffer gas was injected in order to trap and cool the ions (pressure up to 10^{-3} mbar). A time diagram of the sequence of the experiment is presented in Fig. 2. At the end of the accumulation phase, the incident molecular ion jet was blocked by applying a voltage of 25 V to the einzel lens located between the mass filter and the trap, and the He gas injection valve was closed. With the buffer gas off, the pressure in the trap dropped quickly to approximately 10^{-6} mbar in less than 0.5 s of storage time. An ion beam of Xe^{8+} (10 nA) extracted from an electron cyclotron resonance (ECR) source and accelerated to 96 keV was sent into the trap to collide with the stored molecular ions. It was collimated and guided to the center of the trap through a pair of 2.4-mm apertures drilled in two opposite sides of the ring electrode. The number of protonated cyt-C ions stored in the trap was estimated to be on the order of 10^3 ions. Good vacuum condition was therefore necessary to maintain low relative collision cross section (1%) between the Xe^{8+} beam and the background gas composed of residual He gas and neutrals coming from the ESI source. A typical irradiation time of 1.4 s was necessary to deplete about 20% of the stored parent ion population via collision induced charge exchange or dissociation. After the irradiation phase, a pulse of He buffer gas was injected during 0.1 s in order to cool down the energetic dissociation products and quench further dissociation processes. After the whole sequence of accumulation-storage-irradiation-cooling, ±200-V bias voltages were applied to the endcaps of the Paul trap. The stored ions, including intact molecular ions and fragments, were extracted and sent into a time-of-flight (TOF) mass spectrometer of resolution $M/\Delta M \approx 200$. A postacceleration voltage of 5 kV was applied in front of the multichannel plate detector in order to improve the detection efficiency. The detector signal was recorded with a 1-GHz digitizer over 65 μs of TOF range. The typical duration to record a spectrum was about 1 h. In a raw TOF spectrum, peaks due to collisions of Xe^{8+} with the background gas were observed mainly in the low mass-over-charge range below 100 amu. Their contribution to the mass spectra was corrected by the subtraction of a background spectrum obtained without protein accumulation in the trap (see Ref. [28] for details).

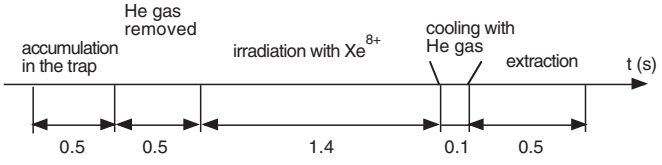

FIG. 2. Time diagram of the experiment.

III. RESULTS AND DISCUSSION

A. Spectrum analyses

Figure 3 shows the mass spectra obtained with or without Xe^{8+} irradiation in experiments using fast Xe^{8+} ions (96 keV) and trapped protonated protein ions cyt-C $[M+18\mathrm{H}]^{18+}$. Figure 4 shows the mass spectra obtained in collisions between Xe^{8+} and cyt-C $[M + q\mathrm{H}]^{q+}$ ($q = 15$–19). In the large mass-over-charge range (500–900 amu), the spectra exhibit only a few peaks showing similar features as the spectra obtained for multiply protonated proteins in ETD experiments [29]. For example, in Fig. 4(a) corresponding to collisions with $[M+15\mathrm{H}]^{15+}$ ions, three main peaks are observed. The dominant peak is assigned to the parent ions $[M+15\mathrm{H}]^{15+}$ and two other peaks at lower mass-over-charge ratio are assigned to

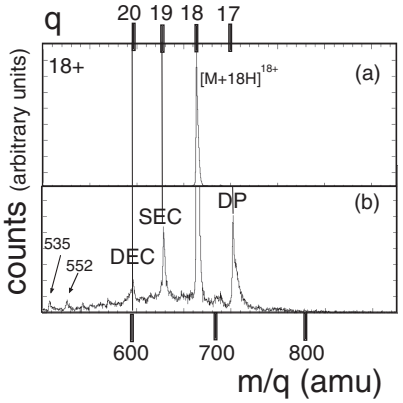

FIG. 3. Mass spectra of trapped protonated cyt-C $[M+18H]^{18+}$ without (a) and with Xe^{8+} ion irradiation (b). SEC, DEC, and DP stand for single electron capture, double electron capture, and deprotonation, respectively. The upper scale indicates the charge of intact molecular ions.

$[M+15H]^{16+}$ and $[M+15H]^{17+}$. Molecular ions undergoing dissociation with the loss of a small neutral fragment could have contributed to the broadening of the observed main peaks. However, in the case of cyt-C, it is expected that dissociation occurs mainly along the backbone leading to the loss of *a*-*b* type or *c*-*z* type fragments [18] with a typical mass large enough to allow the remaining charged fragment to be resolved from the parent ion peak. On the other hand, dissociation of the molecular ions into two or more charged fragments could

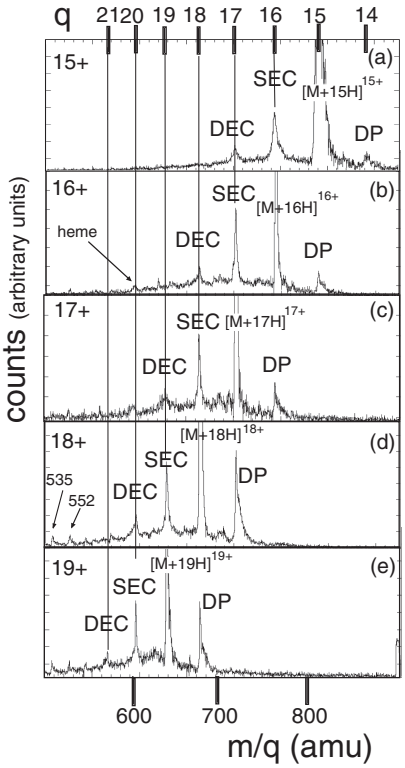

FIG. 4. Mass spectra (a)–(e) in collisions between Xe^{8+} and protonated cyt-C, $[M+qH]^{q+}$ ($q = 15$–19). The upper scale indicates the charge of intact molecular ions.

lead to the production of fragments with mass-over-charge ratio in the domain of our mass spectrum. However, due to the large size of the molecular chain, hundreds of scission sites are possible leading to the broad unresolved background of the spectrum. Therefore, contribution of fragments with the same mass-over-charge ratio as the main peaks is mixed in the background. These arguments allow us to confirm the assignment of the peaks to intact molecules. In all spectra obtained with cyt-C $[M+qH]^{q+}$ $[16 \le q \le 19$; Fig. 4(b)–4(e)], peaks assigned to intact parent ions $[M+qH]^{q+}$ and intact up-charged ions $[M+qH]^{(q+1)+}$ and $[M+qH]^{(q+2)+}$ are observed. We attribute $[M+qH]^{(q+1)+}$ and $[M+qH]^{(q+2)+}$ to single electron capture (SEC) and double electron capture (DEC) processes by Xe^{8+} from the parent molecular ions. Three small fragment peaks can be identified and tentatively assigned. Among these peaks, one corresponds most probably to the monocharged heme molecular ion ($m = 617$ amu) and two others to small monocharged fragments ($m = 535$, 552 amu). To identify precisely all fragment peaks in the background, a mass spectrometer with high mass resolution up to 20 000 would be needed.

Similar as the example shown in Fig. 3(a), mass spectra of the other stored $[M+qH]^{q+}$ ($q = 15$–19) ions have been also measured without Xe^{8+} irradiation. From the spectra normalized to the same experimental conditions, i.e., the same number of trapped ions, the total counts N_{pi} and N_p, of the parent ions $[M+qH]^{q+}$ measured with and without irradiation, have been obtained from the integral of the peaks (Table I). A population depletion ratio of the stored parent ions due to Xe^{8+} irradiation was calculated using $\rho = (N_p - N_{pi})/N_p$ and was found to be $\rho = 17\%$, 19%, 20%, 23%, and 24% ($\pm 1\%$) for $15 \le q \le 19$, respectively. This parameter is related tightly to the total interaction cross section in collisions between Xe^{8+} and $[M+qH]^{q+}$. Typically, higher cross section should lead to larger depletion ratio. The dependency of the measured depletion ratio ρ on q suggests that the total cross section increases slightly with the charge of the protonated molecular ions. From Fig. 4, the counts N_{SEC} and N_{DEC} for the SEC and DEC processes leading to intact molecular ions were measured, respectively, from the integral of the peaks $[M+qH]^{(q+1)+}$ and $[M+qH]^{(q+2)+}$ (Table I). The relative cross section of these processes σ'_{SEC} or σ'_{DEC} was estimated from the ratio of N_{SEC} or N_{DEC} versus the total parent ion population depletion $(N_p - N_{pi})$, $\sigma'_{SEC} = N_{SEC}/(N_p - N_{pi})$ and

TABLE I. Count (integrated area) of each peak after normalization of the spectra. N_p: Parent ion peak $[M+qH]^{q+}$ without irradiation; N_{pi}: Parent ion peak $[M+qH]^{q+}$ with irradiation; N_{SEC}, N_{DEC}, N_{DP}: peaks corresponding, respectively, to single electron capture $[M+qH]^{(q+1)+}$, double electron capture $[M+qH]^{(q+2)+}$, and deprotonation $[M+(q-1)H]^{(q-1)+}$ processes.

q	N_p	N_{pi}	$(N_p - N_{pi})/N_p$	N_{SEC}	N_{DEC}	N_{DP}
15	1216000	1010000	0.17	29000	10000	1600
16	1216000	985000	0.19	23000	6500	11000
17	1216000	973000	0.20	28000	11500	18000
18	1216000	936000	0.23	30000	12500	36000
19	1216000	924000	0.24	28000	10500	49000

$\sigma'_{\rm DEC} = N_{\rm DEC}/(N_p - N_{pi})$. $\sigma'_{\rm SEC}$ was found to vary from 14% to 9% (±1%) with increasing charge q of the protonated molecules $[M+q{\rm H}]^{q+}$ while $\sigma'_{\rm DEC}$ varied slightly with q from 5.0% to 4.0% (±0.5%).

Another intense peak can be observed in the mass spectra of Fig. 4. For instance, in Fig. 4(d) which depicts the results for collisions with $[M+18{\rm H}]^{18+}$, a peak is observed at the nominal mass over charge, 720 amu. This is close to the value expected for the intact molecular ions with a lowered charge, $q = 17+$. Similarly, in spectra obtained with other trapped parent ions $[M+q{\rm H}]^{q+}$, a peak at mass-over-charge ratio around that of the intact molecular ion with a charge q–1 can be also noticed. The calibration of the mass spectra leads to an uncertainty in the mass determination of approximately two to three hydrogen atoms. Furthermore, due to the asymmetric shape of the peak, determination of the mass of the molecular ions with a precision up to the mass of hydrogen is impossible. Nevertheless, in the following, we tentatively attribute these peaks to the quasi-intact parent ions with the loss of one proton, $[M+(q-1){\rm H}]^{(q-1)+}$. This process is labeled DP in Fig. 4 for "deprotonation". This attribution will be discussed in more detail in a following section. From the measured counts $N_{\rm DP}$ (Table I), we have estimated the relative cross section of this process, $\sigma'_{\rm DP} = N_{\rm DP}/(N_p - N_{pi})$. It increases strongly with the charge of the target ions, from about 0.8% (±0.1%) for $q = 15$ to 17% (±1%) for $q = 19$.

The measured SEC, DEC, and DP processes leading to intact or quasi-intact molecules corresponding to about 20% (±2%) to 30% (±2%) $(\sigma'_{\rm SEC}+\sigma'_{\rm DEC}+\sigma'_{\rm DP})$ of the depleted cyt-C $[M+q{\rm H}]^{q+}$ population with increasing charge q. Therefore, a major part of the depleted molecular ions undergoes fragmentation after interaction with Xe^{8+}. A part of the fragmented population contributes to the broad background of the mass spectra and another part may have escaped from the trap. The corresponding relative cross section could be also estimated using $1–\sigma'_{\rm SEC}–\sigma'_{\rm DEC}–\sigma'_{\rm DP}$. It was found to vary from 80% (±2%) to 70% (±2%) with increasing charge q.

B. Calculation of the electron capture distances and total cross sections

In HCI-atom collisions, the electron capture process can be described using the classical over-the-barrier model (COBM) [30] for two approaching point charges. The capture distance estimated with the COBM depends on the charge state of the projectile, the target ionization potential I_p, and the charge state of the target. The COBM has been modified and applied to larger systems such as C_{60} [4] and polycyclic aromatic hydrocarbons [31]. Electron capture dynamics involving biomolecules such as cyt-C are even more complex. Unlike atomic targets or C_{60}, protonated cyt-C targets do not have a spherical symmetry and their conformation depends on the charge state of the molecule. Two examples of conformations are shown in Fig. 5. For high charge states (15+ to 19+), the molecule is expected to exist in a linear extended configuration [Fig. 5(b)], with the length estimated to be $L_p = 20.5$ nm = 388 a.u. In order to estimate the one-electron capture distance and to roughly estimate the total electron capture cross sections using COBM, we considered a simple model called in the following "model total cross section" in which the target

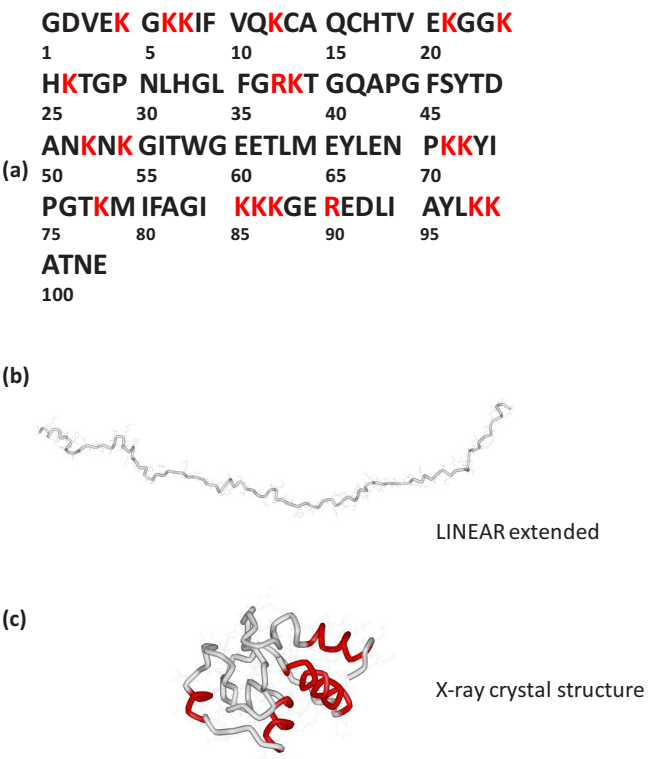

FIG. 5. (Color online) (a) One-letter sequence of bovine cytochrome-C. Alanine (A), arginine (R), asparagine (N), aspartic acid (D), cysteine (C), glutamic acid (E), glutamine (Q), glycine (G), histidine (H), isolucine (I), leucine (L), lysine (K), methionine (M), phenylalanine (F), proline (P), serine (S), threonine (T), tryptophan (W), tyrosine (Y), valine (V). Arginine (R) and lysine (K) basic residues are labeled in red. The numbers indicate the position of residues on the backbone of cyt-C protein from the N terminus. (b) Model structures of cytochrome-C for extended structure assuming dihedral angles of 180° for each peptide bond, followed by structural relaxation using the Assisted Model Building with Energy Refinment force field. (c) Native structure as obtained from x-ray diffraction, taken from the protein database pdb (1CYC).

molecular ion was represented by a linear segment of length L_p along which q positive point charges are distributed at equal distances. For a given collision geometry, we have calculated the electrostatic potential energy curve of an electron escaping from cyt-C $[M+q{\rm H}]^{q+}$ to Xe^{8+} for variable impact parameters. Interactions of the electron with the charge (8+) of the projectile, the charges (q+) distributed along the molecule, and the charge (1+) of the site left by the electron were taken into account. The so-called one-electron capture distance is obtained at a critical impact parameter where the binding energy of the electron in the electrostatic field of the projectile reaches the top of the potential curve. For collisions at shorter distance, the electron transfer from cyt-C $[M+q{\rm H}]^{q+}$ to the approaching Xe^{8+} ion can occur over the potential barrier.

In the following, the center of a molecular target is defined as the origin (O) of a coordinate system (Fig. 6). The z axis is defined by the direction of Xe^{8+} projectile ion beam. We consider in the first step collision geometries [Fig. 6(a)] where the molecule is aligned along the x axis, hence perpendicular

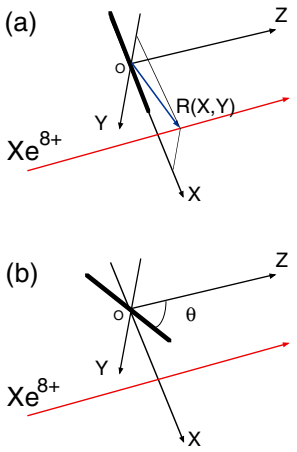

FIG. 6. (Color online) Scheme of geometrical collision configuration.

to the projectile trajectory. For this configuration, the impact parameter is given by $\vec{R} = (X,Y)$. We analyze first the cases where the electron transfer takes place near one of the ends of the molecule. To illustrate the method, we present a particular collision geometry, where the trajectory of the projectile is in the plane Oxz and the impact parameter is given by $(X,0)$ with $X > R_p$. $R_p = L_p/2$ corresponds to the distance between the center and the end of the molecule (194 a.u.). The potential energy curve of the escaping electron along the x axis between one of the ends of the molecule $(R_p,0)$ and the projectile $(X,0)$ was expressed as

$$V(x) = -\sum_i \frac{1}{|x - R_i|} - \frac{8}{|X - x|} - \frac{1}{|x - R_p|}, \quad (1)$$

where R_i stand for the coordinates of protons along the molecular chain. The barrier of the potential energy curve $V(x)$ was estimated for each impact parameter X. It was compared with the binding energy of the electron attached to the end of the molecule in the electrostatic field of the projectile, $-[I_p(q) + 8/|X - R_p|]$. The ionization potential $I_p(q)$ for protonated cyt-C was approximated using a linear relation, $I_p(q) = 11.5 + 0.2q$ eV, obtained by extrapolation of the measurement of Giuliani *et al.* [26]. The capture distance X_c using target molecules with q varying from 15+ to 19+ has been calculated to be 214.6, 214.8, 215.0, 215.2, and 215.4 a.u. corresponding to distances with respect to the end of the molecule X'_c = 17.6, 17.8, 18.0, 18.2, and 18.4 a.u., respectively. For other near-end collisions with impact parameters (X,Y), $X > R_p$, and $Y \neq 0$, comparable distances from the end of the molecules were found. Therefore, the geometrical cross section for the capture of an electron from one end of the molecule is given approximately by $\pi/2X'^2_c$. Considering the two ends of the molecules, the total cross section for electron capture in near-end collisions is given by $S_t = \pi X'^2_c$.

For collision geometries shown in Fig. 6(a), the projectiles pass most probably near the molecular chain with impact parameters $|X| < R_p$, $Y \neq 0$. In such cases, the capture takes place preferentially from the closest amino acid. Along the cyt-C chain, the I_p to remove an electron is not constant. It depends on the specific amino acid from which the electron originates and its distance from the nearby protonated sites. We recall here that the protons are attached preferentially to the basic residues as arginine (R) and lysine (K). Although the tryptophan amino acid has the lowest I_p [32] (letter code W, I_p = 7.44 eV) of all amino acid constituents of cyt-C, it is not necessarily easier to remove an electron from the W site of a highly protonated molecule. Indeed, the W amino acid is close to the neighboring protonated sites and the electron binding energy from this W site could be larger than from some other amino acids. Williams *et al.* [21] have calculated the proton distribution versus the number of protons on cyt-C $[M + q\mathrm{H}]^{q+}$. From that work, one can notice that the amino acid sites with low I_p are those far away from the protonated sites, notably, around residue numbers 32, 45, and 63 [see Fig. 5(a)]. It can be expected that in collisions near these sites, the electron transfer may take place more easily leading to larger capture distance. In collisions close to other sites with slightly larger I_p, the electron transfer is expected to occur at shorter distance. In the present crude model, the above features were not taken into account. The linear relation $I_p(q) = 11.5 + 0.2q$ eV was used as an averaged value without discerning the amino acid or proton sites. The COBM was applied to the case where the projectile passes in the perpendicular bisecting plane between the two most central protons at impact parameter around $(0, Y)$. The electron transfer was estimated to occur at $(0, Y_c)$ at the capture distance $Y_c(0)$ = 28.4, 29.2, 30.2, 31.0, and 31.8 a.u. for the charge q varying from 15+ to 19+, respectively. In order to estimate the electron-transfer cross section, the capture distance $Y_c(X)$ should be estimated for other impact parameters, (X, Y), $-R_p < X < R_p$. As a rough approximation, it was considered as constant along the molecular chain $Y_c(X) = Y_c(0)$, noted as Y_c. Taking into account collisions at both sides of the molecule, the electron capture cross section S_{ch} along the chain was approximated as the surface area of a rectangle of width L_p (length of the molecule) and height $2Y_c$; $S_{ch} = 2Y_cL_p$.

In the second step, we consider collision geometries as shown in Fig. 6(b). A random orientation of the molecular chain in the space is characterized by the angle θ with respect to the z axis. The cross section for collisions along the molecular chain is reduced to $S_{ch}\sin\theta$ while that for near-end collisions S_t can be considered as constant. Making the average over the 4π solid angle, the mean value $<S_{ch}>$ is calculated by the integral, $\frac{1}{4\pi}\int_0^{\pi} S_{ch}\sin\theta\sin\theta d\theta\int_0^{2\pi} d\varphi = \frac{\pi}{4}S_{ch}$. The total cross section σ_{total} including $<S_{ch}>$ and S_t was estimated by $\sigma_{\text{total}} = \pi/4S_{ch} + S_t$. It slightly increases from 35 $\times$ 10^{-14} cm^2 to 40 $\times$ 10^{-14} cm^2 with the charge of protonated cyt-C varying from 15+ to 19+. The increase in the electron capture cross section with the charge of the molecule seems to be counterintuitive. Indeed, due to the Coulomb attraction from protons, it is obviously more difficult to remove an electron from a system with increasing positive charge. This is consistent with the linear increasing dependency of I_p on q. However, this effect is counteracted by the presence of the HCI in the vicinity. In fact, the positive charges along the molecule reduces the potential barrier encountered by the escaping electron and furthermore, the higher the charge of the molecule, the lower the potential barrier. Therefore,

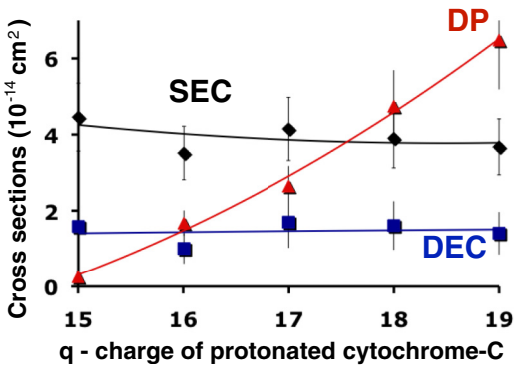

FIG. 7. (Color online) Cross sections for the single (diamonds) and double (squares) capture and deprotonation (triangle) processes versus the charge of protonated cyt-C, $[M+qH]^{q+}$. The lines are to guide the eye.

in the end, the electrostatic field of the highly protonated molecule makes the electron-transfer process a bit easier. This leads to the increase of the over-the-barrier transfer distance with increasing target charge q as evidenced in each of the above impact conditions. Comparing the two analyzed typical cases in impact geometries of Fig. 6(a) with $\vec{R}=(X,0)$ and $\vec{R}=(0,Y)$, at the same collision distance ($X'=X-R_p=Y$) for the same charge q, the potential barrier was found lower for the second case. Indeed, the electrostatic field due to the q protons is stronger along the charged molecular chain than at the end of it. This results in the increase of the capture distance in collisions along the molecular chain leading to $Y_c > X'_c$ for the given q. The variation tendency of the model total cross section σ_{total} with q is in qualitative agreement with the measured increase in the parent ion depletion ratio ρ from 17% ($\pm$1%) to 24% ($\pm$1%) for q varying from 15+ to 19+.

Using the model total cross section σ_{total}, the absolute cross sections for SEC and DEC processes were estimated using the measured relative cross sections, $\sigma_{\text{SEC}}=\sigma_{\text{total}}\sigma'_{\text{SEC}}$ and $\sigma_{\text{DEC}}=\sigma_{\text{total}}\sigma'_{\text{DEC}}$. In Fig. 7, we have plotted σ_{SEC} and σ_{DEC} versus the charge of cyt-C $[M+qH]^{q+}$. Both SEC and DEC cross sections are nearly constant as a function of the charge of the protein.

C. Deprotonation

In Fig. 4, the DP peaks observed at the nominal mass over charge close to the values expected for the intact molecular ions with a lowered charge, $q-1$, are attributed to the deprotonation process, i.e., the loss of a proton leading to $[M+(q-1)H]^{(q-1)+}$. The relative cross section of the DP peaks σ'_{DP} were found to depend strongly on the initial charge of cyt-C $[M+qH]^{q+}$. Using the model total cross section σ_{total}, the absolute DP process cross section versus the initial charge q has been estimated from the measured relative cross sections, $\sigma_{\text{DP}}=\sigma_{\text{total}}\sigma'_{\text{DP}}$ (see Fig. 7). To confirm the attribution of the DP peak to the deprotonation process, other possible mechanisms that may result in a decrease of the precursory parent ion charge state are considered and discussed below:

$$[M+qH]^{q+}+Xe^{8+}\rightarrow[M+qH]^{(q-1)+}+Xe^{9+}, \quad (2)$$

$$[M+qH]^{q+}+Xe^{8+}\rightarrow[M+qH]^{(q+n)+}+Xe^{(8-n)}+ \rightarrow[M+(q-n-1)H]^{(q-1)+}+(n+1)H^{+}+Xe^{(8-n)+}. \quad (3)$$

The first reaction (2) corresponds to single electron transfer from the projectile to the highly protonated protein. Similar charge-decrease process via the capture of an electron by protonated proteins has been observed in collisions with anions [29]. However, in the present case, due to the large ionization potential of about 171 eV for Xe^{8+}, the transfer of a strongly bound electron from Xe^{8+} to $[M+qH]^{q+}$ is highly improbable. Therefore this mechanism is eliminated in the interpretation of the DP peak. The second reaction (3) consists of two steps, i.e., the capture of n ($n=1$ or 2) electrons by the projectile, corresponding to SEC or DEC processes, followed by the loss of $n+1$ protons from the protein. Similar asymmetrical dissociation processes have been observed in collisions between highly charged ions and neutral targets as fullerenes [33–35] or clusters [36]. In the latter cases, multiple electron transfer may lead to the simultaneous excitation of the targets, which is followed by the statistical thermal emission of one or several small charged fragments. The asymmetrical fission of fullerene C_{60} has been observed in collisions with Xe^{8+} projectiles at 80 keV. However, comparing to the intact singly or multiply charged C_{60}, the fission yield amounted to only several percent of the total electron capture cross section. It was attributed to collisions at short impact parameters where a large amount of energy necessary to induce the fragmentation was deposited in the fullerene. Analogous to C_{60}, the loss of $n+1$ protons from $[M+qH]^{(q+n)+}$ should occur in closer collisions with much smaller cross sections than that of intact molecules. If the peak DP was the result of SEC [$n=1$ in the reaction (3)] followed by the loss of $2H^+$, its yield should be expected much smaller than that of the peak SEC. The measured values show, however, the contrary. In Fig. 7 one can see that the cross section σ_{DP} is on the same order of magnitude as σ_{SEC} and at $q=18$ and 19, σ_{DP} is even larger than σ_{SEC}. This very different charge variation tendency of σ_{DP} from σ_{SEC} is in favor of excluding the contribution of reaction (3) to the DP peak, although the fragmentation mechanism after a SEC process and its charge dependency is still unknown. Here, we attribute tentatively the DP peaks observed in Fig. 4 to the deprotonation process,

$$[M+qH]^{q+}+Xe^{8+}\rightarrow[M+(q-1)H]^{(q-1)+}+Xe^{8+}+H^{+}. \quad (4)$$

The deprotonation process is tentatively interpreted as fast ejection of a proton during the collision. Fast ejection of atomic ions has been also observed with significant yield in collisions between Ar^+ at 7 keV and C_{60} [37]. It was interpreted as due to the momentum transfer at short distance between the heavy incident Ar^+ and one of the carbon atoms in head-on collisions. The variation tendency of the measured C^+ yield with the projectile mass and velocity was in good agreement

with the so-called nuclear stopping in collisions with matter. Nevertheless, such direct atomic knock-out type interaction is not in consistence with the observation in the present work. Indeed, short-distance interactions between the projectile ion and randomly one of the atoms of the target should be able to provoke prompt loss of other constituents leading to fragments such as $[M+q\text{H–C}]^{q+}$ or $[M+q\text{H–N}]^{q+}$. Obviously, these peaks are not observed in the mass spectra (Fig. 4). Additionally, the cross section for short-distance head-on collisions should be much smaller than that for the long-distance electron-transfer process and it should be sensitive to the kinetic energy of the collision rather than the charge of the collision partners. In the present experiment, we have observed the contrary. The measured DP cross section increases strongly with the charge of the molecular target and becomes even larger than the SEC cross section for $q = 18$ and 19 (Fig. 7). In order to analyze the role of the projectile charge, we have performed an experiment using Xe^{5+} at 80 keV colliding on trapped cyt-C $[M+16\text{H}]^{16+}$. Although the kinetic energy of the projectile ion beam is equivalent, the yield of the DP peak was found to be significantly reduced in comparison to that obtained in collisions with Xe^{8+}. Hence, the DP peak is characterized by a large cross section and a strong dependency on both the charge of the target molecule and the charge of the projectile. These features suggest that the observed charge sensitive DP process seems to be driven by the long-distance Coulomb interaction between the multicharged incident ion and the protons and it occurs in long-distance collisions rather than in short-distance head-on collisions.

To remove a H^+ from a protonated molecule, the minimum energy cost is given by the apparent proton affinity (A_p^{app}) i.e., the apparent binding energy of the proton. For multiply protonated ions, the apparent binding energy of the proton at site t is specified by $(A_p)_t^{\text{app}}$. Williams and co-workers [21] have proposed the following relation,

$$(A_p)_t^{\text{app}} = (A_p)_{\text{intrinsic},t} - \sum_{i=1,i\neq t}^{q} \frac{1}{R_{i,t}}, \qquad (5)$$

where the first term $(A_p)_{\text{intrinsic},t}$ is the proton affinity of a molecule protonated at site t (the A_p of the basic site in the absence of other charges) and the second term corresponds to the decrease of the binding energy of this proton due to its interaction with the protons at all other sites. We estimated $(A_p)_t^{\text{app}}$ for two extreme conformational cases of a model cyt-C: a native structure (1CYC) based on the x-ray diffraction analysis taken from the protein data base pdb [38] and an extended structure built by setting the two dihedral angles on both sides of each peptide bond to 180°. Views of both obtained structures are shown in Fig. 5. As the peptide sequence of bovine cyt-C contains 20 basic functional groups (see Fig. 5) that can be readily protonated, i.e., 18 lysine (K) and two arginine (R) residues, these groups were considered as the most likely sites for positive charge localization. The distribution of the q charges among these 20 possible sites ($2+ \le q \le 20+$) was then determined for each structure by minimizing the Coulomb energy, $\sum_{i-1}^{q}\sum_{j>i}\frac{1}{R_{i,j}}$, under the assumption that each proton from a basic residue carried a full $+1$ charge. For the minimized distribution, $(A_p)_t^{\text{app}}$ of protons at all occupied sites was calculated with Eq. (5) using a constant value $(A_p)_{\text{intrinsic},t} = 10.4$ eV, corresponding to the proton affinity of lysine residues [21]. The minimum value of $(A_p)_t^{\text{app}}$ was defined as the apparent proton affinity of the molecule, A_p^{app}.

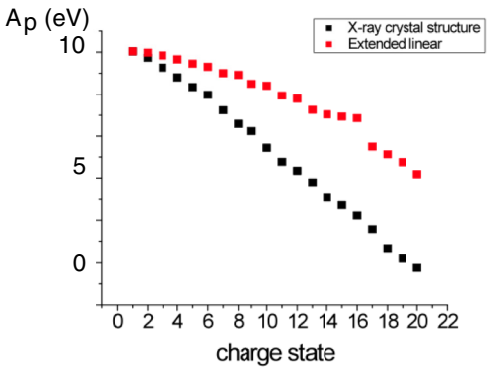

FIG. 8. (Color online) Calculated apparent proton affinity as a function of the charge of protonated cyt-C, $[M+q\text{H}]^{q+}$.

The calculated value of A_p^{app} is plotted in Fig. 8 as a function of q for the two conformations. As expected, the extended linear conformation leads to higher A_p^{app}. The difference between A_p^{app} of native and linear conformations increases from 0.2 to 4.7 eV as the charge q increases from 2+ to 20+. For the native structure, on average, each additional charge lowers A_p^{app} by ~0.6 eV. A negative A_p^{app} value is reached for $q>19$, which corresponds therefore to the maximum charge of this structure. For the extended structure, the decrease of A_p^{app} with q is less important and the value of A_p^{app} remains positive over the whole charge range investigated. These modeled values are in good agreement with those reported by Williams and co-workers [21] using a similar point-charge approach. For the extended configuration, we note also an abrupt decrease of A_p^{app} at charge 16+ and a larger slope in the high charge range. In fact, for $q \ge 16$, extra sites unoccupied at low charge state are involved in the protonation process, for example, the C terminal (103), the P residue (75) and some K residues (12, 54, and 86) (Fig. 5). Some of these sites are located very close to other adjacent protonation sites already filled. Interaction between protons at shorter distance leads to the decrease of $(A_p)_t^{\text{app}}$ of the engaged protonation sites. This explains the fast variation of A_p^{app} with q from 16+ to 19+.

The decrease of A_p^{app} with increasing q is in qualitative agreement with the measured variation tendency of σ_{DP}. Indeed, for molecules in higher charge states, less energy is needed to remove a proton. As a consequence, the proton loss can occur at larger collision distances leading to a larger DP cross section. The underlying mechanism for proton loss, however, is still unclear. A plausible explanation is the following: During the approach of the multicharged projectile, the electronic cloud of the target molecule, which ensures the binding of the nearest H^+, is most strongly polarized. This may lead to a temporary suppression of the binding "barrier" of the proton. As long as the duration for the barrier suppression is comparable to the period of H^+ oscillation, the proton might escape from the parent molecule during the collision.

IV. CONCLUSION

In summary, in collisions between Xe^{8+} and cyt-C $[M+qH]^{q+}$ at 96 keV, for charge state from $q=15$ to 19+, the single and double electron capture (SEC and DEC) processes dominate and leave the protein intact. The cross sections for these processes remain nearly constant with the charge of the protonated cyt-C. The measured population depletion ratio due to ion impact increases with the charge of the molecule showing the same tendency as the electron capture cross section estimated with the over-the-barrier model. Unexpected peaks, $[M+(q-1)H]^{q-1+}$, are observed with increasing cross section for q varying from 15+ to 19+. These peaks are attributed to the deprotonation process, DP, i.e., the loss of a proton from the parents $[M+qH]^{q+}$. The variation of the measured cross section σ_{DP} as a function of q is in good accordance with the calculated proton affinities of cyt-C $[M+qH]^{q+}$ showing a monotonic decrease with increasing charge q. This DP process is tentatively interpreted as due to the temporary barrier suppression for the binding of a H^+ in long-distance interactions between the multicharged projectile and the binding electronic cloud. More experiments using projectile ions at different velocities and charge states would be needed in order to confirm the attribution of the deprotonation process and get more insight on the proton loss dynamics.

[1] M. Barat and P. Roncin, J. Phys. B **25**, 2205 (1992).
[2] H. Bruhns, H. Kreckel, K. A. Miller, X. Urbain, and D. W. Savin, Phys. Rev. A **82**, 042708 (2010).
[3] C. C. Havener, E. Galutschek, R. Rejoub, and D. G. Seely, Nucl. Instrum. Methods Phys. Res., Sect. B **261**, 129 (2007).
[4] H. Cederquist, A. Fardi, K. Haghighat, A. Langereis, H. T. Schmidt, S. H. Schwartz, J. C. Levin, I. A. Sellin, H. Lebius, B. Huber, M. O. Larsson, and P. Hvelplund, Phys. Rev. A **61**, 022712 (2000).
[5] L. Chen, S. Martin, J. Bernard, and R. Brédy, Phys. Rev. Lett. **98**, 193401 (2007).
[6] T. Majima, Y. Nakai, T. Mizuno, H. Tsuchida, and A. Itoh, Phys. Rev. A **74**, 033201 (2006).
[7] B. Manil, L. Maunoury, B. A. Huber, J. Jensen, H. T. Schmidt, H. Zettergren, H. Cederquist, S. Tomita, and P. Hvelplund, Phys. Rev. Lett. **91**, 215504 (2003).
[8] L. Chen, J. Bernard, A. Denis, S. Martin, and J. Désesquelles, Phys. Scr., T **80**, 52 (1999).
[9] J. de Vries, R. Hoekstra, R. Morgenstern, and T. Schlathölter, Phys. Rev. Lett. **91**, 053401 (2003).
[10] P. Moretto-Capelle and A. Le Padellec, Phys. Rev. A **74**, 062705 (2006).
[11] R. Brédy, J. Bernard, L. Chen, G. Montagne, B. Li, and S. Martin, J. Chem. Phys. **130**, 114305 (2009).
[12] F. Alvarado, J. Bernard, B. Li, R. Brédy, L. Chen, R. Hoekstra, S. Martin, and T. Schlathölter, ChemPhysChem **9**, 1254 (2008).
[13] V. Bernigaud, B. Manil, L. Maunoury, J. Rangama, and B. A. Huber, Eur. Phys. J. D **51**, 125 (2009).
[14] S. Bari, R. Hoekstra, and T. Schlatholter, Phys. Chem. Chem. Phys. **12**, 3376 (2010).
[15] S. A. McLuckey and T.-Y. Huang, Anal. Chem. **81**, 8669 (2009).
[16] J. A. Madsen, M. W. Gardner, S. I. Smith, A. R. Ledvina, J. J. Coon, J. C. Schwartz, G. C. Stafford, and J. S. Brodbelt, Anal. Chem. **81**, 8677 (2009).
[17] J. J. Coon, J. Shabanowitz, D. F. Hunt, and J. E. P. Syka, J. Am. Soc. Mass Spectrom. **16**, 880 (2005).
[18] J. J. Coon, B. Ueberheide, J. E. P. Syka, D. D. Dryhurst, J. Ausio, J. Shabanowitz, and D. F. Hunt, Proc. Natl. Acad. Sci. USA **102**, 9463 (2005).
[19] W. Herron, D. Goeringer, and S. Mcluckey, J. Am. Chem. Soc. **117**, 11555 (1995).
[20] M.-S. Kim and A. Pandey, Proteomics **12**, 530 (2012).
[21] P. D. Schnier, D. S. Gross, and E. R. Williams, J. Am. Chem. Soc. **117**, 6747 (1995).
[22] W. Herron, D. Goeringer, and S. Mcluckey, J. Am. Soc. Mass Spectrom. **6**, 529 (1995).
[23] A. R. Milosavljevic, C. Nicolas, J. Lemaire, C. Dehon, R. Thissen, J.-M. Bizau, M. Refregiers, L. Nahon, and A. Giuliani, Phys. Chem. Chem. Phys. **13**, 15432 (2011).
[24] M. Vonderach, O. T. Ehrler, K. Matheis, T. Karpuschkin, E. Papalazarou, C. Brunet, R. Antoine, P. Weis, O. Hampe, M. M. Kappes, and P. Dugourd, Phys. Chem. Chem. Phys. **13**, 15554 (2011).
[25] B. A. Budnik, Y. O. Tsybin, P. Hakansson, and R. A. Zubarev, J. Mass Spectrom. **37**, 1141 (2002).
[26] A. Giuliani, A. R. Milosavljevic, K. Hinsen, F. Canon, C. Nicolas, M. Refregiers, and L. Nahon, Angew. Chem., Int. Ed. Engl. **51**, 9552 (2012).
[27] D. E. Clemmer and M. F. Jarrold, J. Mass Spectrom. **32**, 577 (1997).
[28] S. Bari, R. Hoekstra, and T. Schlatholter, Int. J. Mass Spectrom. **299**, 64 (2011).
[29] G. C. McAlister, W. T. Berggren, J. Griep-Raming, S. Horning, A. Makarov, D. Phanstiel, G. Stafford, D. L. Swaney, J. E. P. Syka, V. Zabrouskov, and J. J. Coon, J. Proteome Res. **7**, 3127 (2008).
[30] A. Niehaus, J. Phys. B **19**, 2925 (1986).
[31] B. O. Forsberg, J. D. Alexander, T. Chen, A. T. Pettersson, M. Gatchell, H. Cederquist, and H. Zettergren, J. Chem. Phys. **138**, 054306 (2013).
[32] F. Gaie-Levrel, G. A. Garcia, M. Schwell, and L. Nahon, Phys. Chem. Chem. Phys. **13**, 7024 (2011).
[33] S. Martin, L. Chen, A. Denis, and J. Désesquelles, Phys. Rev. A **59**, R1734 (1999).
[34] S. Martin, L. Chen, A. Salmoun, B. Li, J. Bernard, and R. Brédy, Phys. Rev. A **77**, 043201 (2008).
[35] S. Martin, L. Chen, A. Denis, R. Brédy, J. Bernard, and J. Désesquelles, Phys. Rev. A **62**, 022707 (2000).
[36] F. Chandezon, T. Bergen, A. Brenac, C. Guet, B. A. Huber, H. Lebius, and A. Pesnelle, Phys. Rev. A **63**, 051201 (2001).
[37] L. Chen, B. Wei, J. Bernard, R. Brédy, and S. Martin, Phys. Rev. A **71**, 043201 (2005).
[38] http://www.pdb.org/pdb/home/home.do.